Astron. Astrophys. 306, 317–325 (1996)

ASTRONOMY AND ASTROPHYSICS

A study of the gravitational wave form from pulsars

K. Jotania[1,2,*], **S.R. Valluri**[3,**], **and S.V. Dhurandhar**[1,***]

[1] Inter-University Centre for Astronomy and Astrophysics, Post Bag 4, Ganeshkhind, Pune 411 007, India
[2] Raman Research Institute, C.V. Raman Avenue, Sadashiva Nagar, Banglore 560 080, India (present adress)
[3] Departments of Philosophy, Math and Physics, University of Western Ontario, London On N6A3K7, Canada

Received 19 April 1995 / Accepted 28 June 1995

Abstract. We present a study of the gravitational wave form from pulsars. Typically the observation times will be of the order of a few months. Due to the rotation and orbital motion of the Earth, a monochromatic signal becomes frequency and amplitude modulated. The effect of both these modulations is to smear out the monochromatic signal into a small bandwidth about the signal frequency of the wave. However, the effect on the Fourier transform of the frequency modulation is much more severe compared to the amplitude modulation in that the height of the peak is reduced drastically. The Fourier transform of the pulsar signal, taking into account the rotation of the Earth for one day observation period is studied. We have obtained an analytical closed form of the Fourier transform considering the rotational motion of the Earth only. With the inclusion of orbital corrections one obtains a double series of Bessel functions.

Key words: gravitation – pulsars – data analysis

1. Introduction

The direct detection of gravitational radiation (GR) from astrophysical sources is one of the most outstanding problems in experimental gravitation today. The rapid variation of spacetime curvature due to, for example, collisions, pulsations or the coherent bulk motion of masses should generate curvature ripples or gravitational waves (GWs) that travel at the speed of light and may carry the identity of the graviton. The construction of large laser interferometric gravitational wave detectors like the Laser Interferometric Gravitational Wave Observatory (LIGO) (Abramovici et al. 1992), the French-Italian gravitational wave observatory VIRGO (Bradaschia et al. 1990; Brillet & Giazotto 1992) and the Australian International Gravitational Observatory (AIGO) (Sandeman et al. 1991) is opening a new window for the study of a vast and rich variety of non-linear curvature phenomena. The network of gravitational wave detectors can in fact confirm that GW exist and by monitoring gravitational wave forms give important information on their amplitudes, frequencies and other important physical parameters. Therefore, the study of different radiative production processes from astrophysical sources and their GW luminosities and dimensionless amplitudes is important.

We can broadly classify the astrophysical sources of GR as continuous, burst type and stochastic. A prototype of a continuous source is a pulsar. If the axis of rotation of a pulsar makes an angle α with the direction of the angular momentum of the pulsar, the resultant time dependent mass quadrupole then becomes the source of GR from such a pulsar. The amplitude of GR from these pulsars is probably very weak ($\leq 10^{-26}$–10^{-28}, for galactic pulsars). The GR signal will be buried deep within the noise of the detector system. The detection of a GR signal therefore warrants the urgent need of careful data analysis with the development of *analytical methods* and *problem oriented algorithms.*

In Sect. 2, we briefly outline the nature of the GW signal from a pulsar, the response of the interferometric detector to GR from a pulsar and the amplitude modulation (AM) of the GW signal. The frequency modulation (FM), the Doppler shift due to rotation and orbital motion of the Earth in the Solar System Barycentre (SSB) frame, its effect on the total phase of the received GW signal and the Fourier transform (FT) of the GW signal are described in Sect. 3. Section 4 contains the summary and concluding remarks.

2. Gravitational radiation from the pulsar

The amplitude h of the GW is given by the formula (Thorne 1987)

$$h = 7.7 \times 10^{-24} \left(\frac{I_{\tilde{z}\tilde{z}}}{10^{45}\,\mathrm{g\,cm^2}}\right)\left(\frac{10\,\mathrm{kpc}}{r}\right)\left(\frac{f}{1\,\mathrm{kHz}}\right)^2\left(\frac{\delta}{10^{-4}}\right), \quad (1)$$

where f is the gravitational wave frequency, r is the distance of the pulsar from the Earth, and δ is the *gravitational ellipticity*

Send offprint requests to: Kanti Jotania
* e-mail address: kanti@rri.ernet.in
** e-mail address: valluri@julian.uwo.ca
*** e-mail address: sdh@iucaa.ernet.in

in the equatorial plane defined as

$$\delta = \frac{\mathcal{I}_{\bar{x}\bar{x}} - \mathcal{I}_{\bar{y}\bar{y}}}{I_{\bar{z}\bar{z}}}, \quad (2)$$

with $\mathcal{I}_{\bar{x}\bar{x}}$ and $\mathcal{I}_{\bar{y}\bar{y}}$ are the components of quadrupole moment along the principal axes in its equatorial plane, $I_{\bar{z}\bar{z}}$ is the moment of inertia of the pulsar about its rotation axis respectively (Thorne 1987). If we assume $\delta_{\rm Crab} \sim 6\times10^{-4}$, $\delta_{\rm Vela} \sim 3\times10^{-3}$ then the h is $\sim 10^{-25}$ and $\sim 10^{-24}$ for the Crab and Vela pulsars respectively. This amplitude is a few orders of magnitude below the sensitivity of VIRGO/LIGO (expected sensitivity $\sim 10^{-23}$). Since the VIRGO/LIGO would make continuous observations over a time scale of a few months or more, a significant enhancement is expected in the signal-to-noise ratio (SNR) by integrating the data over a long interval of time. It should be noted that the VIRGO would be more sensitive in the low frequencies bandwidth (10 Hz–100 Hz) relevant for pulsar search. It offers a much better sensitivity than LIGO. Infact, the latter one suffers from relatively bad seismic isolation (at least for the first generation of the LIGO project).

A detailed analysis of the noise free response of the interferometric antenna to the GR from pulsars has been given by Jotania and Dhurandhar (Jotania & Dhurandhar 1994; Jotania 1994). Our work considers the important effects of both FM and AM in the detection of the GW signal from the pulsar. The GW incident on the detector is assumed to be a monochromatic plane wave having arbitrary direction and polarization (it is known that if the wobble angle between the angular momentum direction and the rotation axis is small then the radiation will be emitted at ω and 2ω where $\omega = \Omega_{\rm em} - \Omega_{\rm pre}$, $\Omega_{\rm em}$ being the electromagnetic frequency, and $\Omega_{\rm pre}$ – the precesion rate (Thorne 1987; Jotania 1994), however here we consider the radiation at the dominant frequency). The response of the detector was calculated using the formalism developed by Dhurandhar and Tinto (Dhurandhar & Tinto 1988) which is based on the Newman-Penrose formalism (Newman & Penrose 1962). In this formalism the wave and the detector are represented by symmetric trace free (STF) tensors and the response is then just the scalar product. Analytic expressions for the wave and the detector tensors in the SSB frame have been given in detail (Jotania & Dhurandhar 1994; Jotania 1994). The response of the detector, denoted as $R(t)$, is given by,

$$R(t) = W^{ij} \cdot D_{ij}, \quad (3)$$

where W^{ij} and D_{ij} are the wave and detector tensors respectively and $R(t)$ is the response of the detector at time t. The $R(t)$ is a linear combination of the two polarizations,

$$R(t) = F_+ h_+(t) + F_\times h_\times(t), \quad (4)$$

where $h_+ = h^{TT}_{XX} = -h^{TT}_{YY}$, $h_\times = h^{TT}_{XY} = h^{TT}_{YX}$ are the GW amplitudes. The antenna pattern F_+ and $F_\times$ are complicated functions of the direction of the incoming wave (θ, ϕ, ψ), the orientation of the detector angles (α, β, γ) (see below), and ϵ which is the angle that the equatorial plane of the Earth makes with the orbital plane of the Earth respectively.

The Euler angles (θ, ϕ, ψ) connect wave axes (X, Y, Z) with the SSB frame axes. The angles (θ, ϕ) give the incoming direction of the wave in the SSB frame. The angle ψ is the polarization angle of the wave, it represents a rotation about the Z-axis (propagation direction of the wave). The angles (α, β) give position of the detector on the Earth. The angle α is the angle the line joining the centre of the Earth to the detector makes with the spin-axis $(z_{\rm E})$ of the Earth, measured from the North pole (α is just co-latitude). The β is the angle between the plane containing the detector position, the centre of the Earth and spin-axis $(z_{\rm E})$ and the $(x_{\rm E}, z_{\rm E})$ plane. This angle β is just the azimuthal angle in equatorial plane of the Earth which keeps changing as the Earth rotates, and γ is the angle the bisector of the detector makes with local meridian. Detailed description about angles can be found in the work of Jotania & Dhurandhar (Jotania & Dhurandhar 1994; for conventions Schutz & Tinto 1987; Goldstein 1980).

The total response is a function of the position of the source, the orientation of the detector on the Earth, the orientation of the spin axis of the Earth and the orientation of the orbital plane. Since the pulsar signal is weak, long integration times $\approx 10^7$ s will be needed to extract the signal out of the noise. Since the detector along with the Earth moves in this time, the frequency of the wave emitted by the source is Doppler shifted. Also the detector has an anisotropic response, the signal recorded by the detector is both frequency and amplitude modulated. We discuss now the two modulations appearing in the response, namely, (i) frequency modulation : in the context of signal detection FM plays a very important role (Sect. 3), and (ii) amplitude modulation.

2.1. Amplitude modulation

The detector possesses a quadrupole antenna pattern. For a given incident wave, a detector in different orientations will record different amplitudes in the response. The functions F_+ and $F_\times$ appearing in the expression of the response (Eq. 4) completely characterise AM for the two polarizations (Jotania & Dhurandhar 1994; Jotania 1994). Since the expressions for F_+ and $F_\times$ are quite complicated, we will consider some special cases to obtain some idea of AM. For the ideal case when the wave is optimally incident on the detector F_+ and $F_\times$ can individually have a maximum value of unity. For a special case when the detector is situated on the equator with arms symmetrically placed about the North-South direction, i.e. $\alpha = \frac{\pi}{2}$, $\beta_0 = 0$, $\gamma = 0$ and the wave given by the parameters $\theta = \frac{\pi}{2}$, $\phi = 0$, $\psi = 0$, the antenna pattern functions F_+ and $F_\times$ are given by,

$$F_+ = \tfrac{1}{2} \sin 2\varepsilon \cos(\omega_{\rm rot} t), \quad (5)$$

$$F_\times = -\cos\varepsilon \sin(\omega_{\rm rot} t), \quad (6)$$

where $\omega_{\rm rot}$ is the rotational frequency of the Earth about its spin axis. For the above case AM results in about 40% drop in amplitude of the signal as compared to optimal incidence (i.e. F_+ or $F_\times = 1$).

3. Study of frequency-modulated pulsar signals

Frequency modulation arises due to translatory motion of the detector acquired from the motion of the Earth. We have only considered two motions of the Earth namely, its rotation about the spin axis and its orbital motion about the Sun. Hence the response is doubly frequency modulated with one period corresponding to one day and the other period corresponding to a year. The FM smears out a monochromatic signal into a small bandwidth around the signal frequency of the monochromatic wave. It also redistributes the power in a small bandwidth. The study of FM due to rotation of the Earth about its spin axis for one day observation shows that the Doppler spread in the bandwidth for 1 kHz signal will be 1.54×10^{-3} Hz. The Doppler spread in the bandwidth due to orbital motion for one day observation will be 1.71×10^{-3} Hz (Jotania 1994). Since any observation is likely to last longer than a day *it will be very important to incorporate this effect in the data analysis algorithms.*

The monochromatic source is frequency modulated by the relativistic Doppler shift:

$$f_{\rm rec} = f_0 \gamma_0 \left(1 + \frac{\boldsymbol{v} \cdot \boldsymbol{n}}{c}\right), \tag{7}$$

where $\gamma_0 = 1/\sqrt{1 - v^2/c^2} \approx 1$, f_0 is the emitted frequency, $\boldsymbol{n}$ is the unit vector from the antenna to the source, $\boldsymbol{v}$ is the relative velocity of the source and antenna (depends directly on source location) and $f_{\rm rec}$ is the frequency received. Consider a source of constant frequency f_0, the FM would then be of the form

$$s(t) = \cos\left(2\pi f_0 t + K \cos(2\pi f_{\rm m} t)\right), \tag{8}$$

where $f_{\rm m}$ is modulating frequency, and K is the modulation index of the signal and we have taken the amplitude of the signal to be unity. The effect of FM on a sinusoidal signal from the source is to generate a forest of sidebands spaced at the modulation frequency. The n-th sideband has an amplitude given by $J_n(f/f_0)$, where J_n is a cylindrical Bessel function of the first kind and the modulation index $K \approx \Delta f/f_0$, and Δf is the spread in the bandwidth of the signal.

In order to study frequency modulation of a monochromatic plane wave, one needs to calculate the Doppler shift due to rotation and orbital motion of the Earth in the SSB frame. For this, we need to know the relative velocity between the source and the detector. The Euler angles (θ, ϕ) give the direction of the incoming wave in the SSB frame. We characterise the motion of the Earth (and detector) in a simple manner:

(a) we assume the orbit of the Earth to be circular.

(b) we neglect the effect of the Moon on the motion of the Earth.

With these assumptions the radial vector $r_{\rm tot}$ in the SSB frame is given by,

$$\begin{aligned} \boldsymbol{r}_{\rm tot}(t) = \Big[& A\cos(\omega_{\rm orb} t) + R\sin\alpha\cos(\omega_{\rm rot} t), \\ & A\sin(\omega_{\rm orb} t) + R\sin\alpha\sin(\omega_{\rm rot} t)\cos\varepsilon - R\cos\alpha\sin\varepsilon, \\ & R\sin\alpha\sin(\omega_{\rm rot} t)\sin\varepsilon + R\cos\alpha\cos\varepsilon \Big], \end{aligned} \tag{9}$$

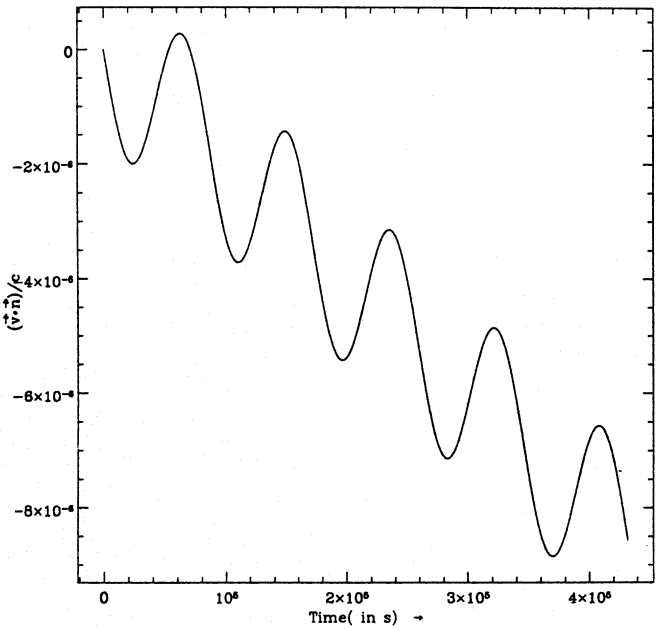

Fig. 1. The Doppler shift variation in the SSB frame due to the rotation and orbital motion of the Earth

where A is distance from the centre of the SSB frame to the centre of the Earth, R is the radius of the Earth, and $\boldsymbol{n}$ is the unit vector in the direction of source, $\boldsymbol{n} = (\sin\theta\cos\phi, \sin\theta\sin\phi, \cos\theta)$. Here we have assumed that at initial time $t_0 = 0$, the longitudinal angle $\beta = 0$. Therefore, the total Doppler shift at time t due to rotation and orbital motion of the Earth in the SSB frame will be,

$$\begin{aligned} \frac{\boldsymbol{v}\cdot\boldsymbol{n}}{c}(t) = \frac{\dot{\boldsymbol{r}}_{\rm tot}(t)\cdot\boldsymbol{n}}{c} = \Bigg[& \frac{A\omega_{\rm orb}}{c}\sin\theta\sin(\phi - \omega_{\rm orb} t) \\ & + \frac{R\omega_{\rm rot}}{c}\sin\alpha\Big[\sin\theta\Big\{\cos(\omega_{\rm rot} t)\cos\varepsilon\sin\phi \\ & - \cos\phi\sin(\omega_{\rm rot} t)\Big\} + \cos(\omega_{\rm rot} t)\sin\varepsilon\cos\theta\Big]\Bigg]. \end{aligned} \tag{10}$$

In Fig. 1 we display a plot of the Doppler shift velocity variation $\frac{(\boldsymbol{v}\cdot\boldsymbol{n})}{c}$. The sinusoidal variation is the diurnal variation and down along the diagonal is the orbital variation which has a periodicity of one year. The phase $\phi(t)$ of the received signal for a single direction sky search (θ, ϕ) is given by,

$$\phi(t) = 2\pi \int_{t_0}^{t} f_{\rm rec}(t')\,{\rm d}t' \tag{11}$$

$$= 2\pi f_0 \int_{t_0}^{t} \left(1 + \frac{\boldsymbol{v}\cdot\boldsymbol{n}}{c}(t')\right){\rm d}t' \tag{12}$$

$$\begin{aligned} = 2\pi f_0 \Bigg[& t - t_0 + \Big\{\frac{A}{c}\sin\theta\cos\phi' \\ & + \frac{R}{c}\sin\alpha\Big\{\sin\theta\big(\sin\beta'\cos\varepsilon\sin\phi + \cos\phi\cos\beta'\big) \end{aligned}$$

$$+\sin\beta'\sin\varepsilon\cos\theta\}\Big\} - \Big\{\frac{A}{c}\sin\theta\cos\phi_0' + \frac{R}{c}\sin\alpha\{\sin\theta(\sin\beta_0'\cos\varepsilon\sin\phi + \cos\phi\cos\beta_0') + \sin\beta_0'\sin\varepsilon\cos\theta\}\Big\}\Big]. \quad (13)$$

where $\phi' = \omega_{\rm orb}t - \phi$, $\beta' = \beta_0 + \omega_{\rm rot}t$, $\phi_0' = \omega_{\rm orb}t_0 - \phi$, $\beta_0' = \beta_0 + \omega_{\rm rot}t_0$, and β_0 is the initial azimuthal angle of the detector at the observation time t_0. It can be seen from Eq. (13) that the Doppler corrections to the phase of the received pulsar signal depends on the direction of the source in the sky.

3.1. *Fourier transform analysis of the FM signal due to the rotational motion of the Earth*

It is instructive to analyse the Fourier transform (FT) of the frequency modulated signal and to study the extent to which the peak of the FT is smudged and how much the FT *spreads* in the frequency space. This type of study would be useful from the point of view of data analysis and for applying such schemes as *stepping around the sky* method (Schutz 1991) which relies on the FT. However, our aim here is modest in that we neglect the Doppler shift due to the orbital motion in studying the FT. Thus a data train up to one day is sufficient for our purpose. We consider the case when the Doppler effect due to the rotation of the Earth is maximal. This is so when the detector is situated on the equator and the direction of the wave is normal to the axis of rotation of the Earth.

When the detector is put on the equator with the arms symmetrically placed about the North-South direction, i.e. $\alpha = \pi/2$, $\beta_0 = 0$, $\gamma = 0$, and the wave parameters given by $\theta = \pi/2$, $\phi = \psi = 0$. The phase $\phi(t)$ is calculated from Eq. (13),

$$\phi(t) = 2\pi f_0 t - x\left[\left(1 - \cos(\omega_{\rm rot}t)\right)\right], \quad (14)$$

where $x = \frac{2\pi f_0 R}{c}$ and we have chosen the initial time instant $t_0 = 0$. Here x plays the role of a modulation index similar to K in the theory of modulation. The modulation index depends on the frequency of the pulsar signal. If we consider only the frequency modulated output of the signal, the output of amplitude unity is given as follows,

$$h(t) = \cos(\phi(t)). \quad (15)$$

We now consider the $h(t)$ to be given on a finite time interval $[0, T]$ which is assumed to be the observation period. In our analysis we have assumed T to be one day. The Fourier transform of the signal $h(t)$ is given by,

$$\tilde{h}(f) = \int_0^T h(t)\,e^{-i2\pi ft}dt. \quad (16)$$

We find it is convenient to use a time coordinate $\xi = \omega_{\rm rot}t$ which for a period of a day is of the order of unity, i.e. when T = 1day = 86400 s, then $\xi_T = \omega_{\rm rot}T = 2\pi$. From Eqs. (15) and (16), we get,

$$\tilde{h}(\nu) = \frac{1}{2\omega_{\rm rot}}\left[I(\nu, x) + I(\nu', x)\right], \quad (17)$$

where

$$I(\nu, x) = \int_0^{\xi_T} e^{i\{\nu\xi - x(1-\cos\xi)\}}d\xi, \quad (18)$$

$$I(\nu', x) = \int_0^{\xi_T} e^{i\{\nu'\xi - x(1-\cos\xi)\}}d\xi, \quad (19)$$

with

$$\nu = \frac{\omega_0 - \omega}{\omega_{\rm rot}},$$
$$\nu' = \frac{\omega + \omega_0}{\omega_{\rm rot}},$$

where ω s are related to the corresponding f s by the 2π factor ($\omega = 2\pi f$). We study the Fourier transform of the frequency modulated signal by three different methods:

(i) Discrete Fourier Transform (DFT) at low frequencies up to 50 Hz. This is due to the limitation of the available core memory on the computer.

(ii) Gaussian quadrature (Gauss-Legendre): This is a numerical integration technique; the limited length of the data train (one day) does not allow fine resolution in the frequency domain. This technique allows us to compute the FT at any desired frequency.

(iii) The analytical approximation: We obtain an approximate expression for the FT.

3.1.1. Discrete Fourier transform

Consider a signal $h(t)$ in the interval $[0, T]$ which is sampled uniformly at N points with sampling interval Δ . The samples are

$$h_k = h(t_k), \quad k = 0, 1, \ldots, N-1, \quad (20)$$

where $t_k = k\Delta$ and $T = N\Delta$. The DFT of the data train is given by

$$\tilde{H}_n = \sum_{k=1}^{N-1} h_k \exp\left(i\frac{2\pi kn}{N}\right), \quad 0 \le n \le N-1. \quad (21)$$

The $\tilde{H}_n$ comprise the DFT of the function h. The FT $\tilde{h}(f)$ is related to the DFT by the relation $\tilde{h}(f_n) \simeq \Delta\tilde{H}_n^\star$ where $f_n = n/T$ are the frequencies at which the DFT is defined and $\star$ denotes complex conjugation. The complex conjugate appears because our convention for the FT is opposite to that of Numerical Recipes (Press et al. 1986) whose routines we have used in our numerical analysis.

There are excellent routines available in the literature to compute the DFT and we make use of these in our analysis. There is the Fast Fourier Transform (FFT) routine based on

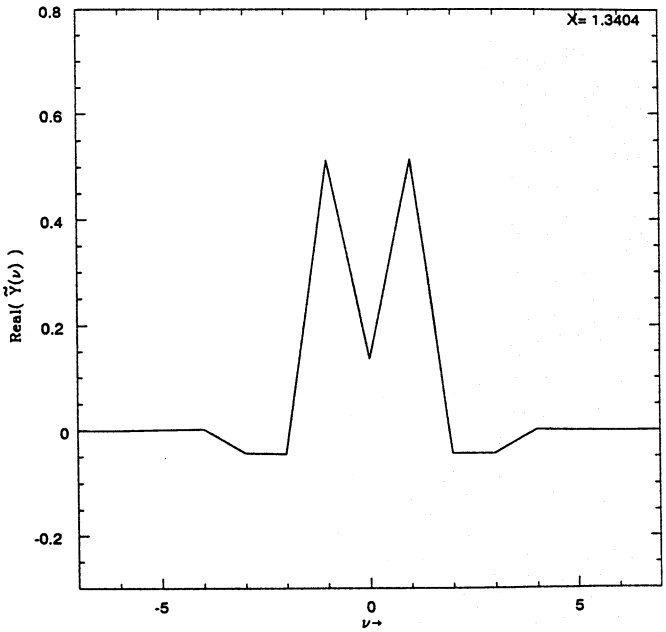

Fig. 2. Normalized DFT of $\cos\phi(t)$ for $f_0 = 10$ Hz

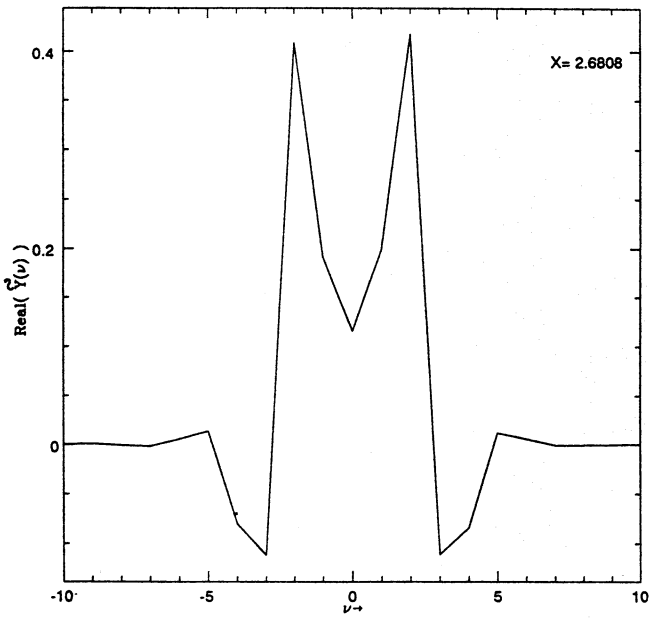

Fig. 3. Normalized DFT of $\cos\phi(t)$ for $f_0 = 20$ Hz

Cooley-Tukey algorithm (Press et al. 1986; Brigham 1988). Since our function is real we use the REALFT routine of Numerical recipes which is appropriate for real functions as compared to the usual FFT routine which is more generally applicable.

We consider the detector orientation and the direction of the wave as mentioned above and take the pulsar signal of frequencies 10.0, 20.0, 40.0 Hz. The corresponding values of x for these frequencies are 1.34, 2.68, 5.36 respectively. In Figs. 2–4, we have plotted the real part of the normalised DFT $\tilde{Y}(\nu)$, as a function of ν and for $\nu > 0$ (There is also a negative frequency

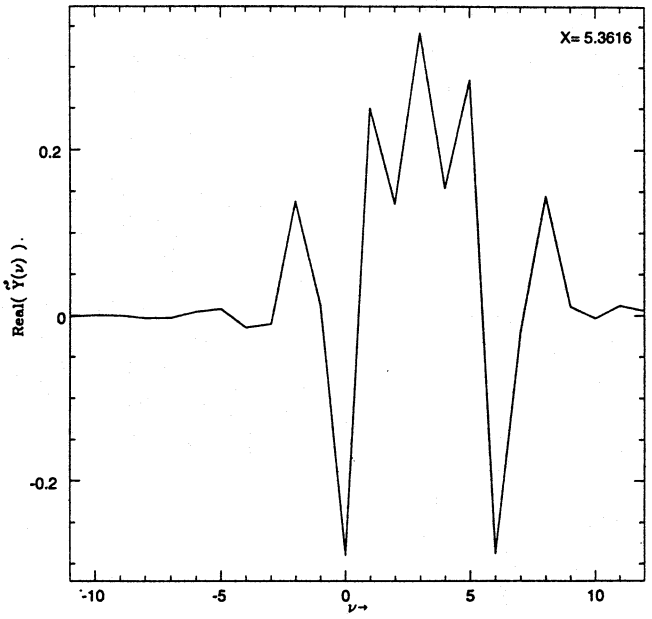

Fig. 4. Normalized DFT of $\cos\phi(t)$ for $f_0 = 40$ Hz

part which is just the mirror image of the positive frequency part). The scale on the vertical axis corresponds to the maximum of the real part of the DFT of the unmodulated signal being unity, i.e. we divide the DFT by the factor $N/2$. The figures showing the normalised FT $\tilde{Y}(\nu)$ are almost symmetric about $\nu = 0$. It is clear that the frequency resolution offered by the DFT is not adequate. At higher frequency, bands generated by Doppler modulation become prominent and thus demand better frequency resolution.

We observe from the figures that the Fourier transform is nonzero only for a small interval of width $2\Delta\nu$ around $\nu = 0$ and rapidly falls to zero outside this interval, $\nu = 0$ correspond to the signal frequency f_0. Also the spread in the Fourier transform is more or less symmetrical about $\nu = 0$. The maximum amplitude of $\tilde{Y}(\nu)$ is seen to decrease from that of the unmodulated signal. We find that the $\tilde{Y}(\nu)$ is oscillatory in nature and maintains roughly a constant amplitude in the interval $[-\Delta\nu, \Delta\nu]$. The frequency of the oscillation is roughly 0.5. We find from the figures, that $2\Delta\nu \sim 3.5$ for 10 Hz, $2\Delta\nu \sim 5.8$ for 20 Hz and $2\Delta\nu \sim 11.0$ for 40 Hz. We observe that the spread $\Delta\nu \sim x$.

One finds that the curves in the figures are not very smooth and one would desire a better frequency resolution when plotting the FT. The frequency resolution of the DFT is $\Delta f = 1/T = 1/86400$ Hz which on the ν-axis corresponds to $\Delta\nu = 1/2\pi$. But this is exactly the scale on which the DFT oscillates as is seen from the figures. Also the scale on the ν axis, $\Delta\nu = 1$ correspond to $\Delta\omega = \omega_{\rm rot}$. Therefore, this resolution on the ν-axis is not adequate to visualise the FT. In order to get a better resolution one could have increased T but this would mean more computational requirements. Instead we choose to use other integration methods for evaluating the FT. We resort to the Gauss-Legendre method which is described in the following subsection.

3.1.2. Gaussian quadrature

The basic idea behind Gaussian quadrature is to find an integration formula of the form (Abramowitz & Stegun 1972; Atkinson 1978)

$$I_n(f) = \sum_{j=1}^{n} w_j f(x_j) \approx \int_a^b w(x) f(x)\,dx = I(f). \qquad (22)$$

The weights w_j and nodes x_j are to be real and the nodes must belong to the interval of integration $[a, b]$. The weight function $w(x)$ should be non-negative, finitely integrable and the integral should be finite. The resulting formulas are extremely accurate and highly reliable. For $w(x) = 1$ on the interval $[-1, 1]$ the Eq. (22) reduces to,

$$\int_{-1}^{1} f(x) \approx \sum_{j=1}^{n} w_j f(x_j), \qquad (23)$$

where x_j's are the zeros of the Legendre polynomial $P_n(x)$, and the weights are

$$w_i = \frac{-2}{(n+1) P_n'(x_i) P_{n+1}(x_{i+1})}, \quad i = 1, 2, \ldots, n. \qquad (24)$$

Eq. (23) is the Gauss-Legendre integration formula. This is a widely known form of Gaussian quadrature integration formula (Abramowitz & Stegun 1972; Atkinson 1978; Press et al. 1986). We use Eq. (14) and GAUSS-LEG routine of Numerical recipes to calculate the FT of the frequency modulated signal. This method has the advantage that one can increase the signal frequency to astrophysically interesting values like $f_0 \simeq 1$ kHz without straining the computability requirements. To perform a DFT for example for a one day observation period the number of points in the data train would have to be at least $86400 \times 2000 \sim 1.7 \times 10^8$. This entails a core memory of hundreds of Megabytes. If we restrict our attention to the interval $2\Delta\nu$ over which the FT is appreciable the Gauss-Legendre method requires less time for computation. Also as seen from the DFT the FT oscillates with a period on the scale of the frequency bins. This method allows us to compute the FT at any desired frequency ν.

We find that to obtain sufficient accuracy for the FT by this method the degree n of the Legendre polynomial $P_n(x)$ should be sufficiently high. The degree n depends on the modulation index x and we find that n should be $\sim 4x$ to get adequate results.

We give below a table (see Table 1) for $x, 2\Delta\nu$, and $\max|\tilde{Y}(\nu)|$ for the signal frequencies 10 Hz, 100 Hz and 1 kHz.

We observe from the table that as the signal frequency increases, the spread $2\Delta\nu$ increases and the height of the FT decreases. The general trend is that $\Delta\nu \approx x$ and $\max|\tilde{Y}(\nu)|$ falls off rapidly. The results of the Gauss-Legendre method are displayed in Figs. 5–9. It can be seen that this method offers adequate frequency resolution for an astrophysically interesting range of frequencies. Numerical results show that for 1 kHz signal and one day observation time, the signal is spread into about 100 bands. It is easy to calculate the number of bands and the reduction in amplitude of the FT using this method. The drop in the amplitude of the FT is roughly proportional to $x^{-1/2}$.

Table 1. Gauss-Legendre method

Frequency	x	$2\Delta\nu$	$\max\|\tilde{Y}(\nu)\|$
10 Hz	1.34	3.1	0.4777
100 Hz	13.4	27	0.273
1 kHz	134	270	0.091

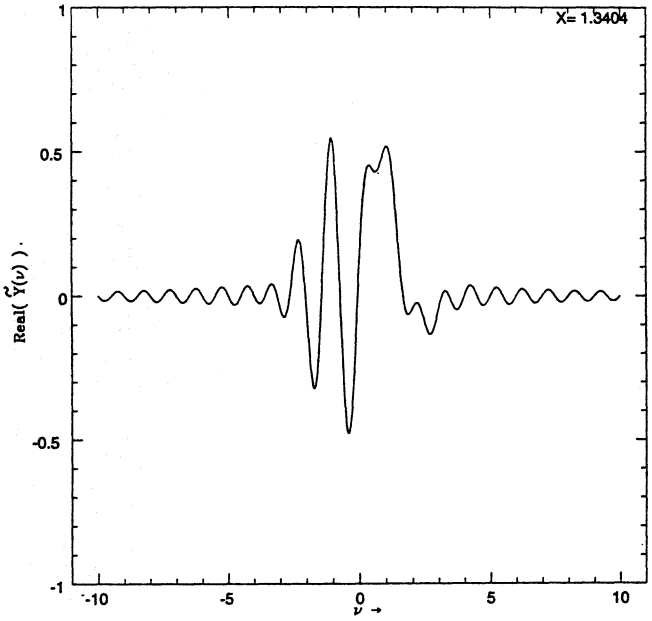

Fig. 5. Normalized DFT of $\cos\phi(t)$ by Gaussian quadrature method for $f_0 = 10$ Hz

In the following subsection we obtain an approximate analytical expression which bears out the above observations.

3.1.3. Analytical approximation

We start with Eqs. (17), (18) and (19). Only Eq. (18) will contribute to the Fourier transform of the Eq. (17). The second term in Eq. (17) will oscillate very fast in the integration limit and it will have very little contribution to the Fourier transform. We have checked numerically the relative contribution of Eq. (19) to the FT. Dropping this term we have,

$$\tilde{H}(\nu) = \frac{1}{2\omega_{\rm rot}} \mathrm{Real}\left\{ e^{-iX} \times \left[\int_0^{\pi} \left(e^{i\nu\xi} e^{iX\cos\xi} + e^{i\nu\xi} e^{-iX\cos\xi} e^{-i\nu\pi} \right) d\xi \right] \right\}. \qquad (25)$$

Using the identity,

$$e^{\pm iX\cos\xi} = J_0(\pm X) + 2\sum_{k=1}^{\infty} i^k J_k(\pm X)\cos k\xi, \qquad (26)$$

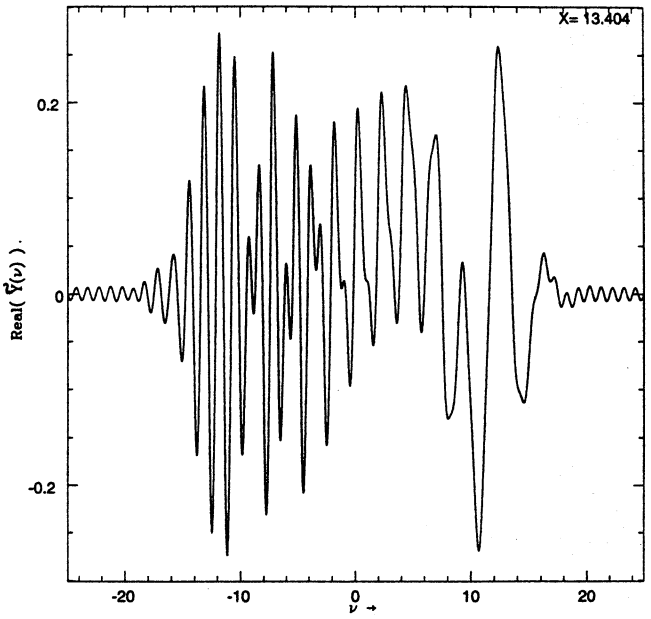

Fig. 6. Normalized DFT of $\cos\phi(t)$ by Gaussian quadrature method for $f_0 = 100$ Hz

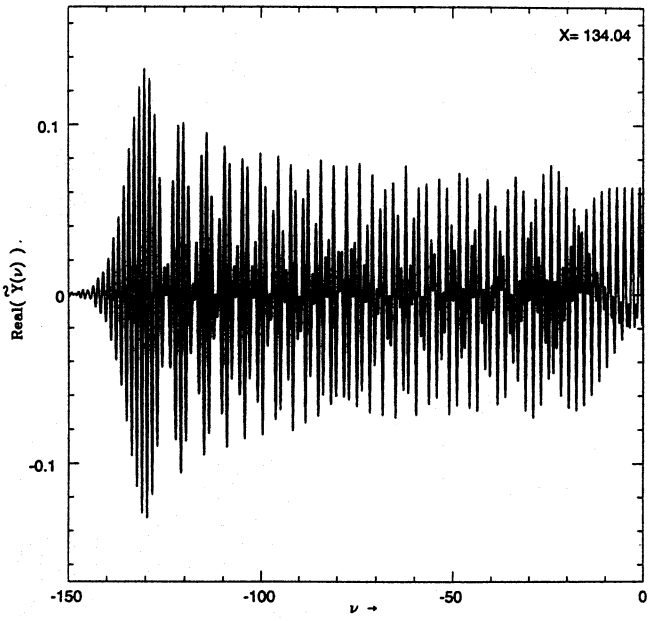

Fig. 8. Normalized DFT of $\cos\phi(t)$ by Gaussian quadrature method for $f_0 = 1$ kHz, Part I

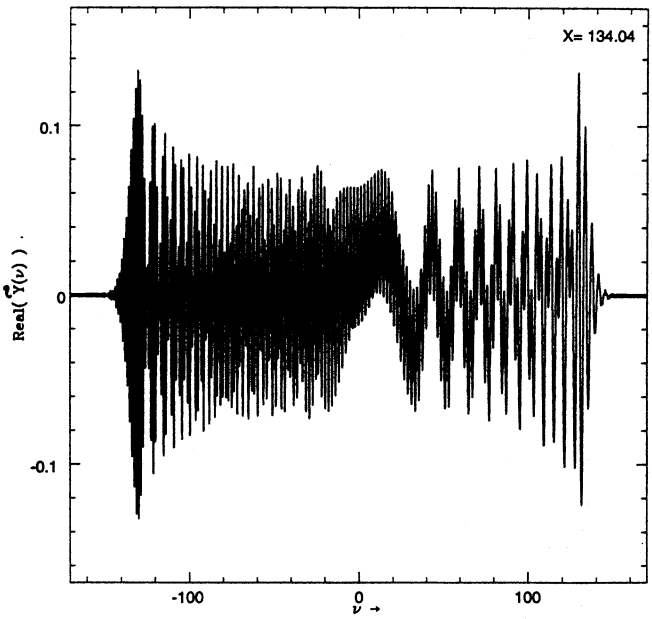

Fig. 7. Normalized DFT of $\cos\phi(t)$ by Gaussian quadrature method for $f_0 = 1$ kHz

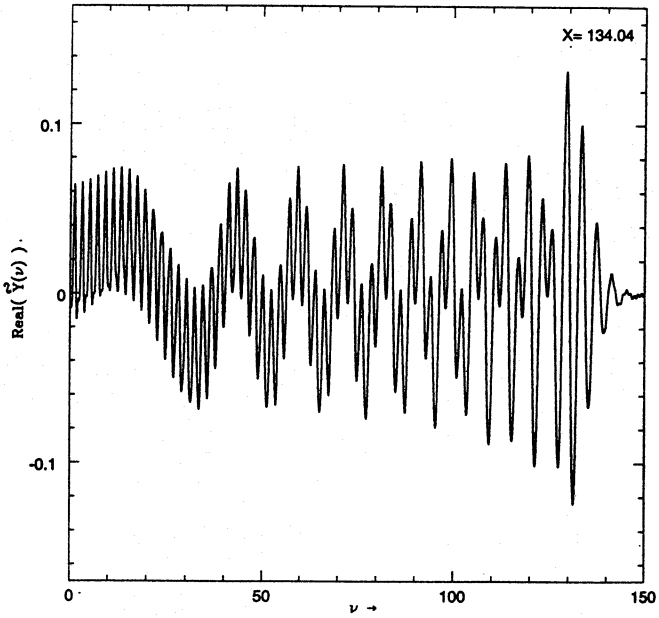

Fig. 9. Normalized DFT of $\cos\phi(t)$ by Gaussian quadrature method for $f_0 = 1$ kHz, Part II

where $J_k(X)$, $k = 1, 2, \ldots, \infty$, is the first kind of Bessel function of integer order k. We have the expression,

$$\tilde{H}(\nu) \simeq \frac{\pi}{\omega_{\rm rot}} \frac{\sin(\nu\pi)}{\nu\pi} \left[J_0(X)\cos X + 2\sum_{k=1}^{\infty} J_k(X)\cos\left(X - \frac{3}{2}k\pi\right)\frac{\nu^2}{\nu^2 - k^2}\right], \quad (27)$$

where we have neglected the fast oscillating term. For $k < X$, (Abramowitz & Stegun 1972),

$$J_k(X) \simeq \sqrt{\frac{2}{\pi}}\left(X^2 - k^2\right)^{-1/4} \times \cos\left(\sqrt{X^2 - k^2} - k\tan^{-1}\left(\frac{X^2}{k^2} - 1\right)^{1/2} - \frac{\pi}{4}\right). \quad (28)$$

For $k > x$,

$$J_k(x) \simeq \left[\frac{k}{x} + \sqrt{\frac{k^2}{x^2} - 1}\right]^{-k} \frac{e^{\sqrt{k^2-x^2}}}{\sqrt{2\pi}\left(k^2 - x^2\right)^{1/4}}. \quad (29)$$

For $k > x$, the $J_k(x)$ decrease very rapidly. Hence the summation in Eq. (27) becomes essentially finite and reduces to,

$$\tilde{H}(\nu) \simeq \frac{\pi}{\omega_{\rm rot}} \frac{\sin(\nu\pi)}{\nu\pi} \Bigg[J_0(x)\cos x + 2\sum_{k=1}^{[X]} \sqrt{\frac{2}{\pi}}\left(x^2 - k^2\right)^{-1/4} \frac{\nu^2}{\nu^2 - k^2} \cos\left(x - \frac{3}{2}k\pi\right) \times \cos\left(\sqrt{x^2 - k^2} - k\tan^{-1}\left(\frac{x^2}{k^2} - 1\right)^{1/2} - \frac{\pi}{4}\right)\Bigg], \quad (30)$$

where $[x]$ is the integer part of x. From this equation it is seen that the amplitude of the Fourier transform drops as $x^{-1/2}$. For the particular values of $\nu = k$, $k = 0, 1, 2, \ldots$ from Eq. (27), we get,

$$\tilde{H}(\nu) = \frac{\pi}{\omega_{\rm rot}} J_0(x) \cos\left(x - \frac{k\pi}{2}\right). \quad (31)$$

The maximum height of the FT of the unmodulated signal is $\pi/\omega_{\rm rot} = \frac{T}{2}$. The factor $J_0(x)\cos\left(x - k\pi/2\right)$ gives the reduction in the height. Hence this analytical approximation explains to a reasonable extent the drop in the amplitude of the FT and spread in the bandwidth due to frequency modulation.

Our ongoing study shows that it is possible to get a closed form of the Fourier transform Eq. (25). It is given by

$$\begin{aligned}\tilde{H}(\nu) = \frac{1}{2\omega_{\rm rot}} {\rm Re}\Bigg\{ & e^{-iX}\frac{\pi}{4}\left(1 + e^{-i2\nu\pi}\right)\left[\frac{\mathbf{J}_\nu(X) + \mathbf{J}_{-\nu}(X)}{\cos\left(\frac{\nu\pi}{2}\right)}\right] \\ & + 2e^{-i(X+\nu\pi)}\left[\frac{\mathbf{J}_\nu(-X) + \mathbf{J}_{-\nu}(-X)}{\cos\left(\frac{\nu\pi}{2}\right)}\right] \\ & + \frac{\pi}{4}e^{i\left(\frac{\pi}{2} - X\right)}\left(1 + e^{-i2\nu\pi}\right)\left[\frac{\mathbf{J}_\nu(X) - \mathbf{J}_{-\nu}(X)}{\sin\left(\frac{\nu\pi}{2}\right)}\right] \\ & + e^{i\left(\frac{\pi}{2} - X - \nu\pi\right)}\left[\frac{\mathbf{J}_\nu(-X) - \mathbf{J}_{-\nu}(-X)}{\sin\left(\frac{\nu\pi}{2}\right)}\right] \\ & + e^{i\left(\frac{\pi}{2} - X\right)}\left(1 - e^{-i2\nu\pi}\right)\Bigg\{\sum_{m=0}^{\infty}\frac{1}{m+\nu}\frac{(iX)^m}{m!} \\ & \times 2F_1\left(-m, 1, 1 - \left(\frac{\nu+m}{2}\right), \frac{1}{2}\right) \\ & - \frac{\pi}{\sin(\nu\pi)}\left[e^{i\frac{\nu\pi}{2}}\mathbf{J}_\nu(X) + e^{-i\frac{\nu\pi}{2}}\mathbf{J}_\nu(-X)\right]\Bigg\}\Bigg\}, \end{aligned} \quad (32)$$

where $\mathbf{J}_\nu(X)$ is the Anger function and $2F_1$ is the hypergeometric series. The details about these functions can be found in literature (Abramowitz & Stegun 1972). To obtain Eq. (32), the Hansen integrals (Erdélyi et al. 1953) have been studied. It is worthwhile mentioning that the integrals of this generic form with $x \to -ix$ have arisen in the theory of X-ray absorption in a magnetic field (Takeuchi 1920). This *closed analytical form of the Fourier transform is a significant contribution to pulsar data analysis* and reduces computational demands.

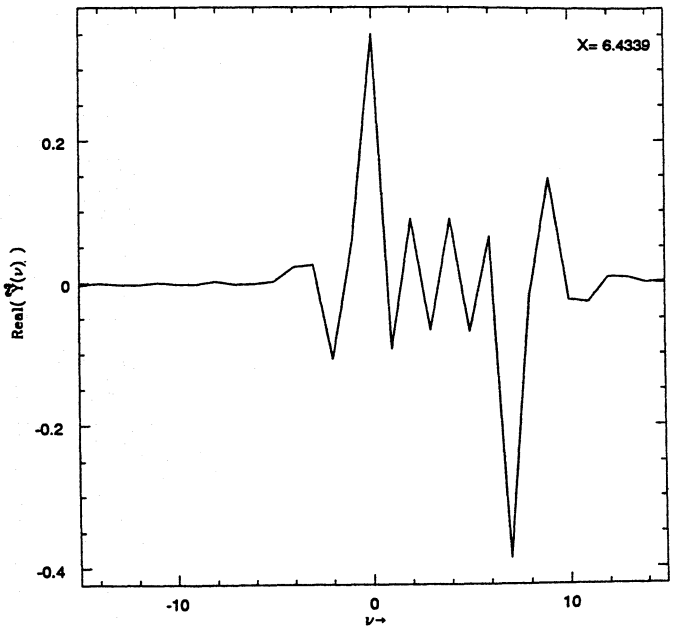

Fig. 10. Smearing of the FT of the frequency modulated signal $\cos\phi(t)$. Here the orbital motion of the Earth has been taken into account

If we include the orbital motion in our analysis, the FT becomes more complex and one obtains a double series of Bessel functions. We need to define the following quantities

$$Y = \frac{2\pi f_0 A}{c}, \quad \text{and} \quad b = \frac{w_{\rm orb}}{w_{\rm rot}} \simeq \frac{1}{365} \simeq 3 \times 10^{-3}.$$

In terms of the above quantities the FT is given by

$$\begin{aligned}\tilde{h}(\nu) = e^{i(Y-X)}\int_0^{2\pi} e^{i\nu\xi}\Bigg\{ & J_0(X)J_0(Y) \\ & + 2J_0(Y)\sum_{k=1}^{\infty} i^k J_k(X)\cos(k\xi) \\ & + 2J_0(X)\sum_{m=1}^{\infty} i^m J_m(-Y)\cos(mb\xi) \\ & + 4\sum_{k=1}^{\infty}\sum_{m=1}^{\infty} i^{k+m} J_k(X) J_m(-Y)\cos(k\xi)\cos(mb\xi)\Bigg\} d\xi. \end{aligned} \quad (33)$$

Figure 10 shows the Fourier transform of the pulsar signal including the orbital motion besides the Earth's rotation about its axis. The distinct bands of the spectrum are clearly seen. Preliminary efforts to look for a closed form expression of the double series indicate that it might be possible.

4. Conclusion

In this paper we have studied the gravitational wave form of a pulsar from the point of view of data analysis. Due to the rotation and orbital motion of the Earth, a monochromatic pulsar signal becomes frequency and amplitude modulated. The effects of these modulations are discussed. The drop in the amplitude of the signal due to the amplitude modulation is about 40% compared to optimal incidence. The effect on the FT of the FM signal is much more severe compared to the AM signal in that the height of the peak is reduced drastically. For example in the case of 1 kHz signal observed for one day, the drop in amplitude of the FT of the signal is 91% (see Table 1). The FM smears out the pulsar signal into a small bandwidth about the signal frequency of the wave. We have studied this frequency modulation of the pulsar signal by three different methods. We have obtained a closed form of the Fourier transform of the frequency modulated pulsar signal due to the rotational motion of the Earth about its spin axis. With the inclusion of orbital corrections one obtains a double series in terms of Bessel functions. This work is a precursor to the all-sky, all-frequency search of pulsars. It would be useful for a scheme like the stepping around the sky method suggested by Schutz (Schutz 1991). Frequency heterodyning is also an important technique to be considered. The number of patches on the sky in the search for pulsars has been estimated (Schutz 1991) to be $\approx 10^{13}$. The sensitivity that can be achieved in an all-sky, all-frequency search is limited by computer technology. Efforts are being made to reduce the number of patches by appropriate analytical methods and initial results are encouraging. A detailed investigation of this problem is presently under study (Srivastva et al. 1995).

Acknowledgements. One of us (S. R. Valluri) would like to thank Natural Sciences Engineering Research Council Canada (NSERC) for an operating grant and the Inter-University Centre for Astronomy and Astrophysics (IUCAA), where this work was carried out, for warm hospitality. We would also like to thank Profs. J. M. Marlborough and R. Mitalas, of the Department of Astronomy, UWO, for helpful suggestions concerning the manuscript.

References

Abramovici A., Althouse W.E., Drever, R.W.P., et al., 1992, Science 256 , 325

Abramowitz M., Stegun I.A., 1972, Handbook of Mathematical Functions. Dover Publication, NewYork, 10th printing with corrections of first edition

Atkinson K.E., 1978, An Introduction to Numerical Analysis. Wiley, NewYork

Bradaschia C., Calloni E., Cobal M., et al., 1991, in: Gravitation 1990, Proc. of the Banff Summer Inst., Banff, Alberta, Mann R., Wesson P. (eds.), World Scientific, Singapore

Brigham E.O., 1988, The Fast Fourier Transform and its Applications. Prentice-Hall, New York

Brillet A., Giazotto A., Jacqemet M., 1992, VIRGO Final conceptual design. Proposed to CNRS/France and INFN/Italy

Dhurandhar S.V., Tinto M., 1988, MNRAS 234, 663

Erdélyi A., Magnus W., Oberhettinger, et al., 1953–1955, Higher Transcendental Functions Vol. II [Bateman Manuscript Project]. McGraw-Hill, New York

Goldstein H., 1980, Classical Mechanics. Addison-Wesley New York, p. 143

Jotania K., 1994, Some Aspects of Gravitational Wave Signal Analysis from Coalescing Binaries and Pulsars, Ph. D. thesis (unpublished)

Jotania K., Dhurandhar S.V., 1994, Bulletin of Astronomical Society of India 22 , 303

Newman E.T., Penrose R., 1962 J. Math. Phy. 3, 566

Press W.H., Flannery B.P., Teukolsky S.A., Vetterling W.T., 1986, Numerical Recipes, The Art of Scientific Computing. Cambridge University Press, Cambridge, England

Sandeman R.J., Blair D.G., Collet J., 1991, Australian International Gravitational Research Centre Proposal to the CRC (University of Western Australia); McClelland D.E. et al., 1991, in: Gravitational Astronomy, McClelland D.E., Bachor H.A. (eds.). World Scientific, Singapore

Schutz B.F., 1991, in: The Detection of Gravitational Waves, Blair D.G. (ed.). Cambridge University Press, Cambridge, England, p. 406

Schutz B.F., Tinto M., 1987, MNRAS 224, 131

Thorne K.S., 1987, in: 300 Years of Gravitation, Hawking S.W., Israel W. (eds.). Cambridge University Press, Cambridge, England, p. 330

Takeuchi T., 1920, Tohuku Mathematical Journal 18, 295

Srivastva D.C., Jotania K., Valluri S.R., 1995 (in preparation)